

Broad band energy distribution of ROSAT detected quasars II: Radio-quiet objects

W. Yuan, W. Brinkmann, J. Siebert, and W. Voges

Max-Planck-Institut für Extraterrestrische Physik, Giessenbachstrasse, D-85740 Garching, FRG

Received February 8; accepted October 7, 1997

Abstract. A database of radio-quiet quasars¹ detected with ROSAT is presented containing 846 quasars seen in the All-Sky Survey and/or in pointed PSPC observations. About $\sim 70\%$ of the objects have been detected in X-rays for the first time. We present the soft X-ray fluxes and spectra, if available. Using an optically selected subsample compiled from this database we study the broad band properties of radio-quiet quasars with high statistical significance.

We confirm that radio-quiet quasars have in general steeper soft X-ray spectra ($\langle\Gamma_{gal}\rangle = 2.58 \pm 0.05$ for $z < 0.5$) than radio-loud objects, with $\Delta\Gamma \sim 0.4$ and $\Delta\Gamma \sim 0.3$, compared to the flat- and steep-spectrum radio quasars (Brinkmann et al. 1997), respectively. The spectral differences persist to high redshifts with $\Delta\Gamma \sim 0.6$ at $z > 2$ compared to flat-spectrum radio-loud quasars. A spectral flattening with redshift is confirmed for the radio-quiet objects up to $z \sim 2$, beyond which the spectral slopes seem to be independent of redshift, similar to that found for radio-loud quasars. The spectral slopes of the ROSAT radio-quiet quasars at $z > 2.5$ ($\Gamma \sim 2.23^{+0.16}_{-0.19}$) are consistent, within the errors, with those found for nearby quasars in the medium energy band (2–10 keV). This implies that X-ray spectral evolution is not important in radio-quiet quasars. We show that there is, in a statistical sense, little or no excess absorption for most of the radio-quiet objects at $z > 2$, in contrast to their radio-loud counterparts.

By dividing the sample into narrow redshift bins, the existence of a correlation between the X-ray luminosity and the luminosity at 2500\AA , i.e., $l_x \sim l_o^e$, is confirmed. Individual objects show a large scatter from this correlation and the slope e takes values in the range $0.75 \lesssim e \lesssim 1.17$, depending on the mathematical method used to analyze the data.

The X-ray loudness α_{ox} appears to be independent of z , but regression analyses indicate a slight increase of α_{ox} with optical luminosity. However, this behavior is, very likely, not caused by physical properties inherent to the quasars but is the result of the intrinsic dispersion of the luminosities and the flux limits in both the optical and X-ray observations.

Finally, we find a small fraction of sources with a substantially larger value of α_{ox} , objects which appear to be relatively “X-ray quiet” compared to the bulk of the other quasars.

Key words: Galaxies: active – quasars; X-rays: general.

1. Introduction

Convincing evidence for a correlation between the X-ray and optical luminosity of quasars, for a surplus of X-ray emission in radio-loud quasars compared to radio-quiet quasars at the same optical luminosity, and for differences in the soft X-ray ($\sim 0.1\text{--}3.5$ keV) spectral properties in the two classes of objects was provided by *Einstein* IPC observations (c.f. Zamorani et al. 1981, Kriss & Canizares 1985, Avni & Tananbaum 1986, Wilkes & Elvis 1987, Canizares & White 1989, Wilkes et al. 1994). Although the samples used were considerably larger than those of previous studies they did not allow an analysis of the X-ray properties of individual subgroups of quasars with sufficient statistical significance. This was especially true for quasars at higher redshifts, where the results were ambiguous because of the small number of detections in X-rays.

The ROSAT observatory (Trümper 1983) provides for the first time the opportunity to study a very large number of quasars in the X-ray domain. More than ~ 30000 AGN are expected to be detected in the ROSAT All-Sky Survey (RASS) of which the majority are not yet optically identified. A correlation of source lists from the ROSAT

Send offprint requests to: W. Yuan

¹ Table I is available in electronic form at the CDS via anonymous ftp to cdsarc.u-strasbg.fr (130.79.128.5) or via <http://cdsweb.u-strasbg.fr/Abstract.html>

All-Sky Survey and from pointed observations with existing catalogues yielded more than 1500 detections of previously known quasars with many of them seen in X-rays for the first time. For the radio-quiet quasars this fraction amounts to about 70%.

In a previous paper (Brinkmann et al. 1997, hereafter paper I), we have presented the data for 574 radio-loud quasars² and 80 quasars detected by ROSAT which show radio emission but either qualify as “radio-quiet” or have no radio-loudness available. Here we present the second part of the ROSAT quasar database—the radio-quiet objects. We give the X-ray flux densities and estimates of the soft X-ray spectral indices, if available, for objects from the RASS (Voges 1992) and pointed observations (ROSAT-SRC, Voges et al. 1995). We present data of detected quasars only, although we will use upper limits for the non-detections in some places in the statistical analyses.

In § 2 we present the data and give details of the derivation of the relevant parameters, and we discuss in § 3 the role of possible X-ray detection biases of the sample. The soft X-ray spectra of the radio-quiet quasars are analyzed in § 4. We then present the relationship between the X-ray and optical luminosity in § 5. Finally, the conclusions are given in § 6.

2. The database of ROSAT detected quasars

We have compiled a database of all radio-quiet quasars from the 6th Véron-Cetty - Véron quasar catalogue (1993, from now on VV93) detected in the RASS, as targets of pointed observations, or as serendipitous sources in pointed observations available publicly from the ROSAT-SRC (Voges et al. 1995). We regard an X-ray source as a detection if the detection likelihood is equal to or greater than 10 as given by the Standard Analysis Software System (SASS, Voges et al. 1992). This threshold corresponds to an about 4σ confidence level. We used an angular distance criterion of $\Delta_{ox} < 60''$ for the cross correlation as in paper I. The total number of ROSAT detected radio-quiet quasars from the above three sources is 846, of which 289 were seen in the RASS only, 385 were only seen in pointed observations, and 172 were seen in both the RASS and in pointed observations. Amongst them are the 69 objects with radio detections, but qualifying as “radio-quiet” according to the above criterion. They have already been presented in paper I.

For all sources from the RASS and pointed observations we use the results of the SASS employing the most recent processing of the Survey data (RASS II, Voges et al. 1996). For objects which have been seen in both, the

² We use $\log R = 1$ as dividing line between radio-loud and radio-quiet objects, where R is the K-corrected ratio of radio to optical flux $R = f(5\text{GHz})/f(2500\text{\AA})$. Objects with $\log R > 1$ are called radio-loud (Stocke et al. 1992, paper I). We used $\alpha_{radio} = 0.5$ and $\alpha_{opt} = 0.5$ for the K-corrections ($S \propto \nu^{-\alpha}$).

ROSAT All-Sky Survey and pointed observations, we take the data from the pointed observations for the determination of the spectral parameters and flux densities, as their statistical errors are considerably smaller due to the generally much longer exposure in pointed observations.

To estimate the X-ray spectral properties and flux densities we assume that the soft X-ray spectrum can be represented by a power law modified by neutral absorption (see paper I for details). For most of the objects the photon indices Γ_{free} and the absorbing column densities N_H , as well as the photon indices assuming Galactic absorption Γ_{gal} (Dickey & Lockman 1990) were estimated using the two hardness ratios given by the SASS with the method described in Schartel (1995) and Schartel et al. (1996). For 134 objects this method did not yield any reliable spectral parameters at all. For another 154 objects we could not determine the photon indices Γ_{free} and the N_H values simultaneously, mostly due to the large statistical fluctuations in the small number of photons accumulated from these sources. Fixing the absorption at the Galactic values yielded, however, proper estimates of the spectral indices Γ_{gal} of the objects. On the other hand, for 9 objects with simultaneous estimates of Γ_{free} and N_H no photon indices assuming Galactic absorption, Γ_{gal} , could be determined.

The X-ray fluxes in the ROSAT band (0.1-2.4 keV) were calculated from the count rates using the energy-to-counts conversion factor (ECF) for a power law spectrum and Galactic absorption (ROSAT AO-2 technical appendix, 1991). We used the photon index obtained for an individual source if the estimated 1σ error of Γ_{gal} is smaller than 0.5, and we took the redshift-dependent average value as derived in §4.1 below for all objects with larger errors.

For objects with more than one pointed observation, the mean values of Γ , N_H , and flux densities as well as their corresponding errors were calculated, assuming that the source did not vary between the different measurements.

In Table 1 we list the relevant information for all 846 quasars. In column 1 we give the IAU designation and, in column 2, a common name. Objects originally detected at other wave bands than in the optical and UV (X-ray, infrared, etc.) are marked with stars; a dagger denotes a quasar found to be radio-loud from recent radio surveys. In a few cases there is more than one quasar apparently associated with an X-ray source within $60''$. We list the most plausible object (mostly the closest) and mark it with a question mark. Furthermore, objects for which the X-ray flux is obviously contaminated by a nearby source (usually extended) are indicated by exclamation marks. Following the optical positions (J2000), we give the redshifts and optical magnitudes, as found in VV93. In column 6 we list the unabsorbed X-ray flux densities in the 0.1 - 2.4 keV energy band. The given errors are the statistical 1σ errors from the count rates only. However, for sources with a small number of counts (mostly from the Survey) the sys-

tematic errors can be of the order of $\sim 30\%$ (see paper I). Further, for strong sources the spectral fits often show that the assumed simple power law slope is an inappropriate representation of the spectrum. In both cases the systematic spectral uncertainties can be considerably larger than the purely statistical errors and the errors given in Table 1 should, therefore, be taken as lower limits. In columns 7 to 10 we give the X-ray power law photon indices and the corresponding N_H values with their 1σ errors, either with free fitted N_H or obtained under the assumption of Galactic absorption. If no error is given, its value is unphysically large. A missing entry means that no reasonable spectral index could be obtained. We used the Galactic N_H values provided by the EXSAS environment (Zimmermann et al. 1994) which are based on an interpolation of data from Dickey & Lockman (1990) and Stark et al. (1992). In column 11 we indicate whether the object was detected in the Survey only (S), in a pointed observation (P), or in both (SP). If published data are available for an object we use these results (mostly spectral indices) if they are of superior quality and we indicate the references in the last entry (column 12).

3. The optically selected quasar sample

In the following we study the broad band energy distribution of radio-quiet quasars using a large optically selected sample only. We compiled this sample from the above database by excluding those quasars which were originally found at other wave bands than the optical (X-ray, infrared, etc.). We also excluded objects without available redshifts, magnitudes, or Galactic column densities, and those with uncertain identifications or with contaminated fluxes. The optically selected radio-quiet sample thus comprises 644 objects, of which 202 were seen in the RASS only, 320 were only seen in pointed observations, and 122 were seen in both the RASS and pointed observations. It should be noted that the sources detected in the Survey form a well defined sample as the Survey's limiting sensitivity is rather uniform (a few times 10^{-13} erg cm $^{-2}$ s $^{-1}$), while the objects we draw from pointed observations clearly form an inhomogeneous, incomplete sample because of the vastly different exposures and thus different observational sensitivities.

There are nearly 5000 optically selected, radio-quiet quasars in the VV93 catalogue not detected either in the RASS or in pointed observations. As shown in paper I, the non-detections in the RASS are mostly due to the X-ray weakness of the sources, with fluxes below the Survey's limiting sensitivity, and only less than 10% of the non-detections can be attributed to source intrinsic variability. Further, some of the non-detections are actually within a small region of the sky where the RASS has a relatively short exposure; for example, about 5% of the non-detections have an exposure less than 100 seconds. A few objects which are associated with ROSAT sources

but at larger angular distances ($60'' \leq \delta_{ox} < 120''$) are not regarded as identifications. We excluded them from the sample of non-detections as well. Since none of the Broad Absorption Line (BAL) quasars has been detected by ROSAT (one possible case has been claimed by Green et al. 1995 and Green & Mathur 1996), and because there is evidence that BAL quasars have soft X-ray properties distinct from the other quasars (Green et al. 1995, Green & Mathur 1996), we excluded them from our analyses. There are thus about 4000 objects with RASS exposures of more than 300 seconds, with available redshifts, magnitudes, and Galactic column densities, which form the subsample of non-detections in our study.

3.1. Sample characteristics

Our sample is based on the VV93 quasar catalogue, which is a compilation of all currently available quasars, and thus it is heterogeneous and incomplete. The sample consists of the cataloged optically selected quasars without radio detection. For optically faint objects this does not necessarily mean that they are radio-quiet as the radio emission of some of them might fall below the sensitivity limits of the currently available radio surveys. Using the above dividing line $\log R = 1$, objects fainter than $B \sim 18$ magnitude (i.e., a large fraction of objects in the sample, see Fig. 1) will be classified as radio-loud if their radio flux is greater than ~ 1 mJy—a value below all current radio survey flux limits. In other words, even objects as bright as ~ 15 th magnitude might erroneously be classified as radio-quiet, because they remain undetected in the currently most sensitive large scale radio surveys, i.e. the 87GB survey ($f_{5\text{GHz}} \gtrsim 20\text{mJy}$; Gregory & Condon 1991) and the Parkes-MIT-NRAO (PMN) survey ($f_{5\text{GHz}} \gtrsim 25\text{mJy}$; Gregory et al. 1994) of the southern hemisphere. For example, the cross correlation of the VV93 radio-quiet sources with the PMN radio survey yielded 55 objects, which are thus radio-loud; 5 of them were detected by ROSAT (marked with daggers in Table 1) and excluded from the analysis. Similarly treated were 12 objects from a recent quasar correlation with the NVSS survey (Bischof & Becker 1997). However, we still expect most of the quasars without radio detection to be radio-quiet because of the generally low fraction of radio-loud objects ($\sim 15\%$, Kellermann et al. 1989) among optically selected quasars.

3.2. Detection biases

We plot in Fig. 1 the cumulative number-magnitude diagram for the whole optically selected, radio-quiet quasar sample (squares), for all the objects detected by ROSAT in the RASS or in pointed observations (triangles), and those seen in the RASS only (circles). For illustrative purpose we show as a dashed line the slope for uniformly populated sources in Euclidean space, normalized at magnitude $B = 16$. The curve for the RASS detected sources

flattens already at $B \sim 16$ due to the limited sensitivity of the X-ray survey, which results in a lower X-ray detection rate at the faint end of the magnitude distribution compared to the total sample. The inclusion of objects detected in pointed observations greatly enlarges the size of the sample of X-ray detected quasars, especially at fainter optical magnitudes. However, it does not improve substantially the completeness of the sample of X-ray detections as the accumulated area of the pointed observations covers only $\sim 10\%$ of the sky.

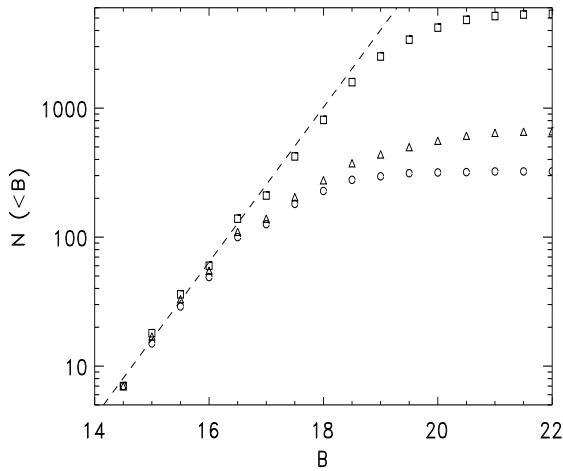


Fig. 1. The number-magnitude diagram for the whole optically selected, presumably radio-quiet sample in the VV93 quasar catalogue (squares), the ROSAT detections from the RASS or pointed observations (triangles) and the objects detected in the RASS only (circles). The dashed line is the slope (normalized at $B = 16$) for uniformly populated sources in Euclidean space for illustrative purpose.

The ROSAT All-Sky Survey has a relatively uniform limiting sensitivity of a few $\times 10^{-13}$ erg cm $^{-2}$ s $^{-1}$ with the exact value depending slightly on the amount of intervening Galactic absorption, on the exact shape of the X-ray spectrum of the source, and on the local Survey exposure. In Fig. 2 we plot the detection rate (in percent) of the RASS for the radio-quiet quasars (hatched) as a function of magnitude, i.e., the number of objects detected in the RASS in a magnitude bin divided by the total number of objects at that magnitude in VV93. Objects with exposures in the RASS of less than 300 seconds are excluded. For comparison the detection rate for the radio selected radio-loud sample (see paper I) is also presented. Apart from the flux limit of the Survey, the detection probability at a given magnitude depends on the ratio of the flux densities in the X-ray and optical wave bands. Beyond 16 mag, the continuous decrease of the detection rate with increasing B over about 3 magnitudes suggests a sub-

stantial dispersion of the optical flux density (a factor of ~ 16) for the RASS objects with an X-ray flux at the Survey limit, and thus, a large dispersion in the ratio of the X-ray-to-optical flux densities for radio-quiet quasars. This implies a similar dispersion of the luminosity ratios between the X-ray and optical wave bands, the X-ray loudness, since the effect of different K-corrections in the two wave bands is small (a factor of $1+z$ for the typical optical and X-ray spectral indices of $\alpha = 0.5$ and 1.5 , respectively, $S \propto \nu^{-\alpha}$). We will study the X-ray-to-optical luminosity ratio quantitatively in detail in § 5. It is noted that even at very bright optical magnitudes ($B \sim 15$) there exist a number of objects which remain undetected in the RASS and which must thus have very low X-ray-to-optical flux ratios. Some of them, detected later in pointed observations, show unusually weak soft X-ray fluxes relative to their optical emission compared to the bulk of the optically selected quasars, and will be discussed in §5 below.

Large differences in the detection probabilities can be seen between the radio-loud and radio-quiet quasars. The radio-loud quasars have X-ray detection rates significantly higher than radio-quiet objects at a given optical brightness, and they are detected at much fainter optical magnitudes (down to ~ 21 mag). Given the average X-ray-to-optical luminosity ratio found previously (Wilkes et al. 1994, Green et al. 1995, paper I) radio-loud quasars are X-ray brighter than radio-quiet objects by a factor of $\sim 3-4$. If we reduce artificially the measured X-ray luminosities of the radio-loud objects by this factor, taking into account the appropriate K-corrections, we find that many of them would not have been detected in the RASS and the detection probabilities of the radio-loud and radio-quiet quasars would then roughly match. This means that the different detection probabilities are mainly caused by the differences in the X-ray-to-optical luminosity ratios between the two classes.

In Fig. 3 the detection rate is shown as a function of redshift. The most distant radio-quiet quasar detected in the RASS is 0053-2532 at redshift $z = 2.70$, however, with a relatively large angular distance of $\sim 50''$ between the X-ray and optical position and a high X-ray-to-optical luminosity ratio of $\alpha_{ox} \sim 1.0$ (see §5 for α_{ox}). The X-ray detection rate of radio-quiet quasars drops much faster towards higher z than that of radio-loud objects, and no sources are found in the RASS at $z > 3$. In contrast, radio-loud quasars were seen in the RASS up to very high redshifts ($z \sim 4$), and the detection rate appears to increase towards higher redshifts. However, this increase might not be statistically significant as the total number of radio-loud quasars at $z \geq 2.5$ is 48 of which 20 were detected (cf. Paper 1).

In Fig. 4 we show the K-corrected broad band soft X-ray luminosities (0.1–2.4 keV) of the sources in our sample as a function of redshift (see § 5 for details of the calculation of the luminosities). We have used a Friedman cosmology with $H_0 = 50$ kms $^{-1}$ Mpc $^{-1}$ and $q_0 = 0.5$ for the com-

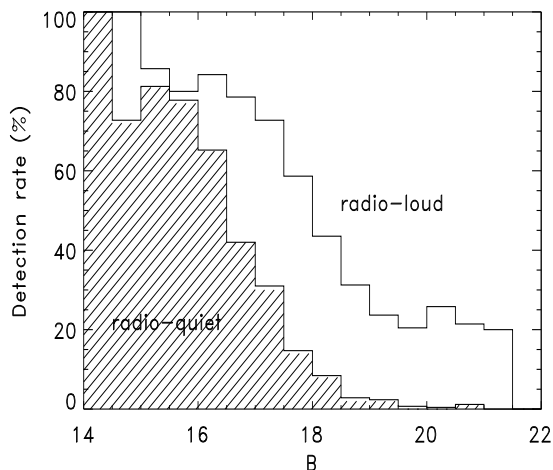


Fig. 2. Detection rate in percent of quasars in the RASS as a function of optical magnitude for both radio-quiet (hatched) and radio-loud (open) quasars.

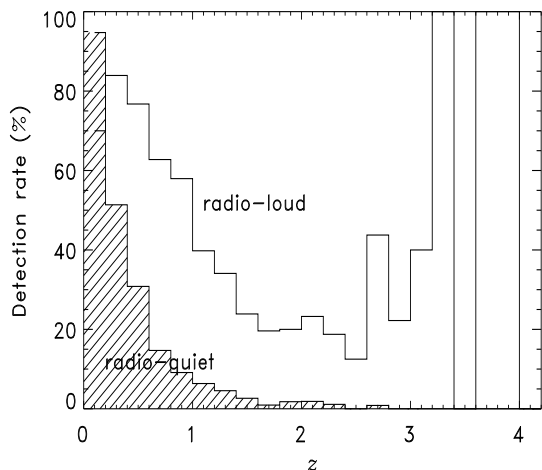


Fig. 3. Detection rate in percent of quasars detected in the RASS as a function of redshift for both radio-quiet (hatched) and radio-loud (open) quasars.

putation of the luminosities. For illustrative purposes we plot (full curve) the K-corrected luminosity corresponding to the typical Survey detection limit of 4×10^{-13} $\text{erg cm}^{-2} \text{s}^{-1}$. It shows that many sources have luminosities definitely below the Survey's sensitivity limit and they could thus be detected only in pointed observations.

3.3. Variability

More than 100 quasars have been observed repeatedly in pointed observations and they thus provide a good sample for an evaluation of the X-ray variability of quasars.

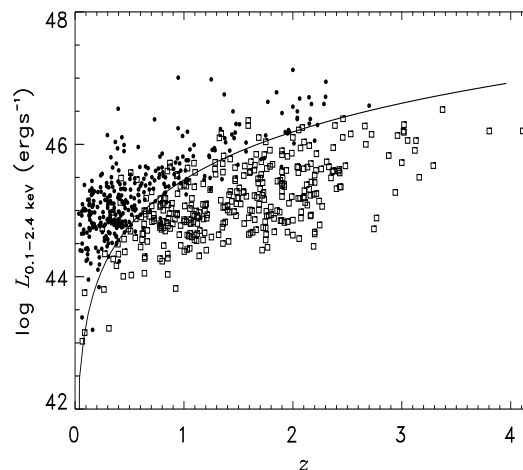


Fig. 4. Integrated X-ray luminosity (0.1–2.4 keV) as a function of redshift for the radio-quiet quasar sample. Filled circles are sources seen in the RASS, and open squares are objects detected in pointed observations only. The full curve represents the K-corrected luminosity of a source at the typical Survey flux limit of 4×10^{-13} $\text{erg cm}^{-2} \text{s}^{-1}$.

In Fig. 5 we plot a histogram of the observed maximal variability of the objects, i.e., the ratio between the highest and the lowest count rates. The distribution of the count rate ratio follows approximately a Gaussian with a $\sigma \sim 0.5$, which is indicated by the dashed curve in the figure. Similar to the radio-loud sample, Fig. 5 shows that a large fraction of the quasar population is variable, mostly by less than a factor of two in flux. For weak sources low intrinsic variability cannot be distinguished from statistical fluctuations. No extremely variable quasars (by a factor of 5 or more), as found in the radio-loud sample in paper I, seem to exist. However, if we compare the X-ray fluxes of sources observed in pointed observations with the corresponding RASS fluxes, for which the uncertainties are larger, we do find one case of extreme flux variation by a factor of six (PG 0844+349) with a count rate of $\sim 0.568 \pm 0.04$ (413 s exposure) in the RASS and $\sim 0.095 \pm 0.003$ in the pointed observation, respectively. Interestingly, no statistically significant spectral changes were found between the two observations and the X-ray spectrum is not particularly steep ($\Gamma \sim 2.5 \pm 0.1$). Unfortunately, as most of the repeated observations of a source have been performed in different ROSAT pointing periods we cannot make any reliable estimates about the variability time scales and the relation between the time scale and variability amplitude of a source.

4. X-ray spectra of radio-quiet quasars

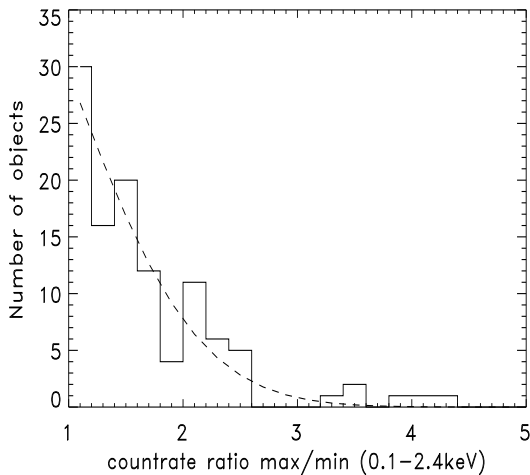


Fig. 5. Histogram of the variability of quasars seen more than once in pointed observations. The ratio of the highest and the lowest observed count rates is used as a measure of flux variability. The dashed curve is the best fit of a Gaussian distribution.

4.1. Mean spectral indices

Spectral studies of radio-quiet quasars in the medium energy range yielded power law slopes $\langle\Gamma\rangle = 1.90 \pm 0.11$, $\sigma = 0.20^{+0.16}_{-0.12}$ in the 2–10 keV band observed by *EXOSAT* (Lawson et al. 1992) and $\langle\Gamma\rangle = 2.03 \pm 0.16$, $\sigma = 0.13^{+0.17}_{-0.06}$ (90% confidence) in the 2–20 keV band observed by *Ginga* (Williams et al. 1992). In the softer energy range quasars show a wide variety of spectral indices with a mean $\langle\Gamma\rangle \sim 2$ (0.2–3.5 keV) from *Einstein* IPC observations (Wilkes & Elvis 1987, Canizares & White 1989). In the even softer ROSAT PSPC energy band (0.1–2.4 keV), spectral studies of quasars generally give steeper spectra ($\Delta\Gamma \sim 0.5$) and a wider dispersion of the indices than found in the harder energy band (Brinkmann 1992, Brunner et al. 1992, Fiore et al. 1994, Schartel et al. 1996, Laor et al. 1997). This steepening of the power law slopes is commonly explained by an additional soft component in the ROSAT PSPC bandpass (see Mushotzky et al. 1993 for a review), similar to that seen in Seyfert I galaxies (Turner & Pounds 1989, Masnou et al. 1992, Walter & Fink 1993). Radio-loud quasars are found to have systematically flatter spectral indices than radio-quiet objects over the total X-ray range, by $\Delta\Gamma \sim 0.3$ in the 2–10 keV energy band (Lawson et al. 1992, Williams et al. 1992), $\Delta\Gamma \sim 0.5$ in the 0.2–3.5 keV band (Wilkes & Elvis 1987, Canizares & White 1989), and $\Delta\Gamma \sim 0.2 - 0.3$ in the 0.1–2.4 keV band (Brunner et al. 1992, Schartel et al. 1996, paper I). An extra hard X-ray component which is linked to the radio emission of radio-loud quasars might be an explanation for this differences in spectral indices.

We used a maximum-likelihood method described in Maccacaro et al. (1988) and Worrall & Wilkes (1990) to

estimate the intrinsic distribution of the power law photon indices, assuming that both the distribution of the indices and the uncertainties of the measurements are Gaussian. To minimize possible redshift effects, we split up the sample into different redshift ranges, as defined in Table 2. We considered only objects for which both indices, Γ_{free} and Γ_{gal} , are available. For a few objects with extremely small errors of the measured spectral indices due to very high photon statistics we use a lower bound for the systematic uncertainties of $\delta\Gamma = 0.05$ to avoid the large statistical weight of individual strong sources. Further, in many cases a simple power law is usually not a good representation of the soft X-ray spectrum for these objects. The best estimates of the mean and standard deviation (errors are at joint 68% confidence level for two parameters) are listed in Table 2. We plot the best estimates (crosses) and the 90% confidence contours in Fig. 6 for objects at both low ($z < 0.5$) and high ($z > 2$) redshifts, for the power law indices Γ_{free} obtained with free N_H (solid line) and for the indices Γ_{gal} obtained with fixed Galactic N_H (dashed line), respectively.

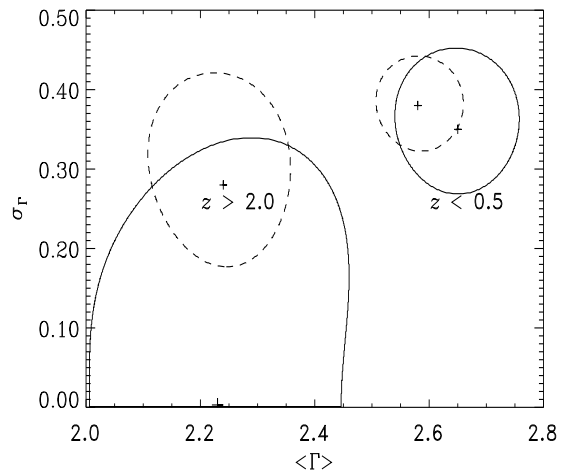


Fig. 6. Best estimates (crosses) and 90% confidence contours of the mean $\langle\Gamma\rangle$ and dispersion σ of the photon index distribution for the $z < 0.5$ and $z > 2$ objects. Solid curve: $\langle\Gamma_{free}\rangle$ obtained with free absorption; dashed curve: $\langle\Gamma_{gal}\rangle$ obtained with absorption fixed at the Galactic column density.

The two mean spectral photon indices $\langle\Gamma_{free}\rangle$ and $\langle\Gamma_{gal}\rangle$ are compatible with each other within their 1σ errors, implying a general agreement between the value of the absorbing column density determined from fitting the X-ray spectra and the Galactic value from HI radio measurements at all redshifts. For objects at $z < 0.5$ the mean photon index ($\langle\Gamma_{gal}\rangle = 2.58 \pm 0.05$, $\sigma_{gal} = 0.38^{+0.04}_{-0.04}$) is in good agreement with that found by Schartel et al. (1996; $\langle\Gamma_{gal}\rangle = 2.54 \pm 0.04$, $\sigma_{gal} = 0.24 \pm 0.03$).

Table 2. Mean spectral photon index and dispersion in different redshift bins

redshift	number	$\langle\Gamma_{free}\rangle$	σ_{free}	$\langle\Gamma_{gal}\rangle$	σ_{gal}
$z < 0.5$	146	$2.65^{+0.08}_{-0.08}$	$0.35^{+0.07}_{-0.06}$	$2.58^{+0.05}_{-0.05}$	$0.38^{+0.04}_{-0.04}$
$0.5 \leq z < 1.0$	81	$2.54^{+0.16}_{-0.16}$	$0.31^{+0.16}_{-0.16}$	$2.46^{+0.07}_{-0.07}$	$0.34^{+0.06}_{-0.05}$
$1.0 \leq z < 2.0$	107	$2.36^{+0.13}_{-0.14}$	$0.20^{+0.16}_{-0.15}$	$2.35^{+0.06}_{-0.06}$	$0.34^{+0.06}_{-0.05}$
$z > 2.0$	56	$2.23^{+0.15}_{-0.15}$	$0.00^{+0.20}_{-0.00}$	$2.22^{+0.09}_{-0.09}$	$0.28^{+0.10}_{-0.08}$
$z > 2.5$	15	$2.20^{+0.53}_{-0.53}$	$0.00^{+0.61}_{-0.00}$	$2.23^{+0.16}_{-0.19}$	$0.26^{+0.20}_{-0.12}$

Note: errors are at joint 68% confidence level for 2 parameters

At high redshifts ($z \gtrsim 2.5$), the energy band of the X-ray spectrum measured with ROSAT corresponds to a rest frame energy of up to ~ 10 keV, similar to the *EXOSAT/Ginga* bandpass for observations of low redshift objects. We found $\langle\Gamma_{gal}\rangle = 2.23^{+0.16}_{-0.19}$ and $\sigma_{gal} = 0.26^{+0.20}_{-0.12}$, in good agreement with Bechtold et al. (1994b) who give $\langle\Gamma_{gal}\rangle = 2.15 \pm 0.14$ using a sample of 6 objects from ROSAT pointed observations. The mean spectral slope and dispersion at $z \gtrsim 2.5$ are consistent, within $\sim 1\sigma$ errors, with those found for low redshift quasars by *EXOSAT* ($\langle\Gamma\rangle = 1.90 \pm 0.11$, $\sigma = 0.20^{+0.16}_{-0.12}$; Lawson et al. 1992) and *Ginga* ($\langle\Gamma\rangle = 2.03 \pm 0.16$, $\sigma = 0.13^{+0.17}_{-0.06}$, 90% confidence; Williams et al. 1992). The marginal difference of the mean spectral indices could result from the lower bound of the source intrinsic energy range in the ROSAT observations (~ 0.4 keV for quasars at $z = 2.5$, compared to ~ 2 keV for *EXOSAT* and *Ginga* for local quasars). Thus, the spectral slopes in the intrinsic energy range up to 10 keV for high and low redshift quasars are comparable, which implies that X-ray spectral evolution is not important in radio-quiet quasars. The steep spectra of radio-quiet quasars seen at high redshifts strengthen the claims that they cannot be the dominant contributors to the cosmic X-ray background, unless their spectra flatten substantially at higher energies (Fabian & Barcons 1992). However, they may have a considerable contribution to the possible “soft excess” of the cosmic X-ray background at softer energies (Hasinger et al. 1993, Gendreau et al. 1994).

The results confirm the long established difference of spectral indices between the radio-loud and radio-quiet quasars at low redshifts (Wilkes & Elvis 1987, Canizares & White 1989, Brunner et al. 1992). Radio-quiet quasars show steeper power law spectra by $\Delta\Gamma \sim 0.4$ and $\Delta\Gamma \sim 0.3$ compared to the flat- and steep-spectrum radio quasars (paper I), respectively. This difference persists and gets even larger at redshifts $z > 2$ by $\Delta\Gamma \sim 0.6$.

4.2. Redshift dependence of spectral indices

ROSAT studies of quasars revealed a flattening of the spectral slope with increasing redshift both for radio-loud (Schartel et al. 1992, Schartel et al. 1996, paper I) and

for radio-quiet objects (Stewart et al. 1994). This trend is found to disappear at redshifts higher than $z \sim 2$ for the radio-loud quasars (paper I). The spectral indices at these redshifts, for which the observed energy band corresponds to ~ 0.3 –7 keV in the quasar’s rest frame, are consistent with those found for nearby objects in the medium energy band by *EXOSAT* and *Ginga*. The aforementioned composite continuum spectrum of quasars (Stewart et al. 1994, Schartel et al. 1996), which consists of a hard component seen in the medium energy band and a steep component at softer energies can account for this effect in that the soft component moves out of the ROSAT energy band with increasing redshift. This photon index – redshift dependence has been modeled by Schartel et al. (1996) by fitting a two-component spectrum to the data of radio-loud quasars.

It can be seen in Table 2 that the mean photon index flattens progressively with increasing redshift. In Fig. 7 we plot Γ_{gal} as a function of redshift for a subsample of 488 quasars for which the determined photon indices Γ_{gal} have errors of $\delta\Gamma_{gal} < 1.0$. A Spearman rank correlation test yields a correlation coefficient $R_s = -0.29$ ($N=488$) which corresponds to a probability for such a correlation to occur by chance of $P_r \simeq 3 \times 10^{-11}$ for the whole subsample, and a probability of $P_r \simeq 5 \times 10^{-6}$ for the $z \leq 2$ objects, indicating a correlation with redshift at a high significance level. However, the correlation weakens significantly and even disappears at higher redshifts: for $z > 2$ we find $R_s = -0.09$ ($N=70$), $P_r = 0.45$, and for $z > 2.5$, $R_s = 0.15$ ($N=17$), $P_r = 0.58$, respectively. In the $z \leq 2$ range a regression analysis without weighting yielded the relation $\langle\Gamma_{gal}\rangle = 2.63(\pm 0.04) - 0.20(\pm 0.04) \times z$, as indicated by the dashed line in Fig. 7. At $z > 2$ the mean $\langle\Gamma_{gal}\rangle$ is $\sim 2.22 \pm 0.09$ (see Table 2, the conventional mean without weighting is ~ 2.19), which is indicated by the horizontal dashed line in the figure. The choice of the break redshift in the above analysis is somewhat arbitrary, but it seems to be around $z \sim 2$. Furthermore, in Table 2, there seems to be a progressive decrease in the dispersion σ_{gal} of the intrinsic distributions of spectral slopes with increasing redshift, though all values are consistent within their 1σ errors.

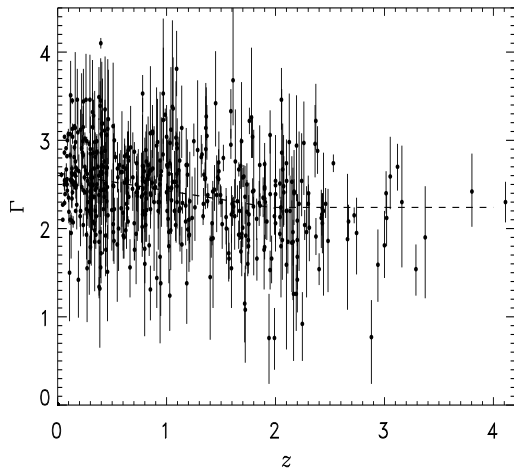


Fig. 7. X-ray photon index Γ_{gal} as a function of redshift for radio-quiet quasars detected by ROSAT. The resulting linear regression line is indicated as a dashed line (see the text).

We thus confirm a flattening of the soft X-ray spectra with increasing redshift for our large sample of radio-quiet quasars. This trend is found to vanish beyond a redshift of ~ 2 , similar to that found for the radio-loud quasars (paper I). The continuity of the spectral flattening with redshift, as seen in Table 2 and Fig. 7, supports the two-component model of the soft X-ray spectrum of quasars. The wide range of the power-law indices implies that the soft excess component varies from object to object and in time, which is supported by observations of individual objects (Elvis et al. 1991, Masnou et al. 1992). The cutoff at redshift of ~ 2 suggests that the soft excess contribution to the X-ray continuum becomes negligible above ~ 0.3 keV in the quasar’s rest frame. The similarity in the spectral index–redshift relation between radio-loud and radio-quiet quasars suggests a similar origin of the soft X-ray emission in these two object classes.

4.3. Absorbing column density

Previous studies of quasars with the *Einstein* IPC gave no indications for intrinsic excess absorption (Canizares & White 1989, Wilkes & Elvis 1987). For low redshift quasars, ROSAT observations confirmed these results showing good agreement between the absorbing column densities obtained from spectral fits and those inferred from HI observations (Schartel et al. 1996, Laor et al. 1997). Recent analyses of ROSAT and ASCA observations of high- z ($z \gtrsim 3$) radio-loud quasars reveal, however, that excess absorption is common in these objects (Elvis et al. 1994, Siebert et al. 1996, Cappi et al. 1997, and paper I) and might even be temporarily variable (Schartel et al. 1997). Radio-quiet quasars probably do not show this effect (Bechtold et al. 1994a), which indicates that this ex-

cess absorption is intrinsic to the radio-loud quasars, but the statistics on which this argument is based is poor. The search for absorption in radio-quiet quasars is hampered by the fact that for most of the high- z objects observed by ROSAT not enough photons could be accumulated for a precise determination of the spectral parameters for the individual object. Furthermore, even if there exists excess absorption it will mainly affect the lower part of the spectral energy band which will be redshifted out of the ROSAT bandpass if the absorber is at high redshifts as well. This usually results in large uncertainties in the determination of the absorbing column density. However, the large number of objects at high redshifts available in Table 1 allows a statistical analysis of the presence of this excess absorption in our sample.

For a statistical test the mean value of the differences between the fitted and the Galactic column densities, $\Delta N_H = N_H - N_{H,gal}$, is difficult to evaluate because the fitted N_H values are asymmetrically distributed with respect to the actual $N_{H,gal}$, with a longer tail towards higher N_H values. For example, the simple method to calculate the mean by assuming a normal distribution usually gives an overestimate for the mean. This problem is even more severe in the case of data with poor statistical quality, which results in large uncertainties in the deduced N_H values.

We used an indirect, yet simple, non-parametric statistics to test for the presence of excess absorption. We assume that there is no systematic discrepancy between the X-ray measured column densities and the radio HI results, and that there are no systematic errors in the measurements. If there were no intrinsic absorption in any quasar the distribution of ΔN_H should have a mean of zero and a median not greater than the mean. For a sample in which the data are obtained with high statistical significance, the distribution is approximately symmetric and the median would be close to the mean. Then, if the hypothesis of “no excess absorption” is true, the median of ΔN_H should not be greater than zero, or, equivalently, the number of objects with $\Delta N_H \leq 0$ (denoted as Σ) should not be smaller than half of the total sample, with scatter caused by the uncertainties of the X-ray measurements. We use the quantity Σ as a test statistic (binomial test, one-tail) to test the hypothesis. We ignored objects for which the corresponding $N_{H,gal}$ values are higher than $5 \times 10^{20} \text{ cm}^{-2}$ as at these values the fitted spectral parameters tend to have large uncertainties in the PSPC energy band. We also ignored objects with large errors in the fitted absorption column ($\delta N_H > 2 \times 10^{21} \text{ cm}^{-2}$). This yielded 340 objects for which N_H values could be fitted, which were further divided into four redshift bins, as defined in Table 3. The number of objects in each bin, the median of the normalized $\Delta N_H / N_{H,gal}$, the Σ value, and the corresponding probability levels P that the corresponding subsample is drawn from a parent population without excess absorption are listed in the upper panel of Table 3.

Table 3. Results of the binomial test for no excess absorption

subsample	number	median	$\Sigma^a)$	$P^b)$
$z < 0.2$	53	0.01	25	0.34
$0.2 \leq z < 1.0$	142	0.14	62	0.06
$1.0 \leq z < 2.0$	98	0.22	40	0.04
$z \geq 2.0$	47	0.40	15	0.006
objects with > 100 photons				
$z < 0.2$	45	0.01	21	0.33
$0.2 \leq z < 1.0$	79	0.03	39	0.45
$1.0 \leq z < 2.0$	41	0.01	19	0.32
$z \geq 2.0$	13	0.16	5	0.23

a) number of objects with $\Delta N_H \leq 0$

b) the probability level that the sample is drawn from a parent population without excess absorption

The data are consistent with no or little excess absorption at low redshifts, in agreement with what has been found in previous studies. At high redshifts ($z \geq 2$) the data seem to suggest a surplus in the column densities obtained from the X-ray data, though the significance is not very high. We have checked the possibility that the differences result from different $N_{H,gal}$ distributions for the objects at high ($z \geq 2$) and low redshifts ($z < 0.2$). The two $N_{H,gal}$ distributions are consistent with each other (χ^2 test, with a reduced $\chi^2 = 0.87$ for 9 d.o.f). Further, no correlation is found between the obtained ΔN_H and $N_{H,gal}$ in our data. A plausible explanation might be the low photon statistics in some of the high-redshift quasars for which only relatively few photons could be accumulated.

We thus restrict our analysis to objects with more than 100 source counts and list the result in the lower panel of Table 3. For $z \geq 2$ objects the probability level is reduced to 0.23 only, and the data are consistent with no excess absorption. The previously derived P including objects with low numbers of source photons is thus, at least partly, an artifact of systematic biases. Unfortunately, the small size of the sample (with more than 100 source photons) makes such a test rather insensitive when the fraction of objects with possible “excess absorption” is small. More observational data for high- z radio-quiet objects are needed in order to obtain results with higher statistical significance.

We conclude that the current data are, in a statistical sense, consistent with no or only little excess absorption at all redshifts for radio-quiet quasars, in contrast to their radio-loud counterparts, which show a high incidence of excess absorption at higher redshifts. At redshifts beyond $z = 2$ more observational data are needed for radio-quiet quasars.

5. Broad band energy distribution

The knowledge of the exact form of the relation between the X-ray and optical luminosities is required to relate the quasar statistics (evolution, luminosity function) in the two wave bands and to understand the quasars’ broad band emission. The X-ray-to-optical energy distribution is commonly characterized by α_{ox} , the broad band spectral index from the ultra-violet (2500Å) to the X-ray (2 keV) which is defined as the luminosity³ ratio $\alpha_{ox} = -0.384 \log (l_{2\text{keV}}/l_{2500\text{Å}})$. A dependence of the X-ray luminosity of the form $l_x \sim l_o^e$ is equivalent to the relation $\alpha_{ox} \sim \beta \log l_o$ with $e = 1 - 2.605 \times \beta$.

Previous studies of optically selected quasars gave the following results: α_{ox} is nearly independent of redshift but it increases with l_o , or equivalently, there exists a non-linear relationship $l_x \sim l_o^e$ with $e \sim 0.7 - 0.8$ (Kriss & Canizares 1985, Avni & Tananbaum 1986, Wilkes et al. 1994, Avni et al. 1995). Using ROSAT survey data for the Large Bright Quasar Survey sample, Green et al. (1995) found a similar non-linear relationship. For models of a pure luminosity evolution of quasars, this implies a slower luminosity evolution in X-rays than in the optical. Interestingly, there are recent reports suggesting a linear relationship $l_x \sim l_o$ and, consequently, α_{ox} being independent of l_o (La Franca et al. 1995). The results were achieved by applying a regression analysis to the *Einstein* data which takes into account the errors in both variables.

Using the large sample of ROSAT detected radio-loud quasars and similar regression methods, Brinkmann et al. (paper I) also found a linear relationship $l_x \sim l_o$ for a subsample ($29.6 < \log l_o < 31.7$) of flat-spectrum quasars and a marginally flatter slope, $e \sim 0.94 \pm 0.13$, for the whole sample of both flat- and steep-spectrum quasars. But the existence of an X-ray component related to the radio emission in radio-loud quasars introduces additional complications in the analysis. Radio-quiet quasars, therefore, seem to be better suited to study the relationship between the optical and X-ray emission, which is believed to originate from the active nucleus.

We convert the observed X-ray fluxes into luminosities as in paper I. For the K-correction and the calculation of the monochromatic X-ray luminosity, the individual spectral index for an object is used if it is obtained with relatively small error ($\delta \Gamma < 0.5$), otherwise the redshift dependent mean spectral index derived in § 4 is used. For the subsample of non-detections, we estimated the upper limits for the source count rates using the local RASS exposure at the optical positions of the objects and assume less than 12 source photons from the objects. This assumption is based on the fact that almost all sources which were found with a detection likelihood less than 10 have less than 12 source photons. For a source within

³ In the following, we will for convenience refer to the luminosity $l_{2500\text{Å}}$ as to the “optical luminosity”, l_o .

a background of strong diffuse X-ray emission or in the vicinity of another strong X-ray source, this estimate for the upper limit might not be correct. However, we expect that such cases are rather rare and that they do not affect our statistical results. Furthermore, for sources showing abnormally weak X-ray emission compared to their optical brightness, we have visually checked the RASS source images to avoid possible inappropriate estimates of upper limits. For more than 100 objects which were found with detection likelihoods ≥ 7 ($\approx 3\sigma$) in the RASS but lower than our threshold of 10 and which were thus not regarded as detections, we used the measured count rates as upper limits. In the optical band, the B magnitudes are taken from the VV93 catalogue. We apply an extinction correction using the fitted relation between reddening and Galactic column density for a constant gas-to-dust ratio (Burstein & Heiles 1978). Magnitude corrections due to emission lines were made as described in Marshall et al. (1983). The luminosities at 2500\AA are calculated by assuming an optical spectral index $\alpha = 0.5$.

In § 5.1 we study the luminosity correlation between the optical and X-ray bands. Then we investigate the distribution of the X-ray-to-optical luminosity ratio α_{ox} in § 5.2, and a study of its dependence on z and l_o is presented in § 5.3.

5.1. Luminosity correlations

The proper treatment of redshift effects is one of the biggest difficulties in the investigation of luminosity correlations. As our sample is relatively large, we are able to minimize these effects by using objects within a narrow redshift bin. For the analysis we consider objects with $z < 1$ only, since at $z \gtrsim 1$ the low fraction of X-ray detections of our sample ($\lesssim 5\%$, see Fig. 3) can hardly yield reliable results. We split the redshift range $z = 0.1 - 1.0$ into 9 bins with a bin size of 0.1. The changes of the luminosity distance square within a redshift bin of $\Delta z = 0.1$ are about factors of 4 and 1.2 at $z = 0.15$ and $z = 0.95$, respectively, which is small compared to the corresponding range of luminosities of more than one order of magnitude. The objects within a single redshift bin can thus be regarded as being at approximately the same distance.

For the subsample of each z bin we tested the $l_x - l_o$ correlation, using a Spearman correlation test incorporating upper limits (using the survival analysis software ASURV; Rev 1.3, LaValley et al. 1992). The probability level for rejecting the “no correlation” hypothesis, P_r , ranges from 0.47×10^{-2} to 0.11×10^{-5} , with a median of 0.84×10^{-3} for all nine subsamples. The weakest correlation ($P_r = 0.47 \times 10^{-2}$) occurs in the lowest redshift bin, $z = 0.1-0.2$, where the intrinsic luminosity range is rather small ($\log l_o = 29.8 - 30.6 \text{ erg s}^{-1} \text{ Hz}^{-1}$). We thus confirm the correlation between l_o and l_x being an intrinsic property for most objects of the quasar population at redshifts $z = 0.1 - 1$, rather than a distance or a selection

effect. However, despite the presence of a significant correlation the data points show a rather large scatter around the regression line. Part of the scatter in the low- z ($\lesssim 0.5$) bins, which show relatively large P_r values, comes from a few objects showing rather weak X-ray luminosities compared to their optical luminosities ($\alpha_{ox} \gtrsim 2.0$), deviating from the rest of the subsample. Excluding objects with $\alpha_{ox} > 2.0$ (for details see § 5.2) yielded generally reduced P_r values except in the $0.1 \leq z < 0.2$ bin.

As an example, we plot in Fig. 8 the $l_x - l_o$ relationship for the subsample in the $z = 0.3 - 0.4$ bin, in which the upper limits of the X-ray luminosities for the non-detections (47 out of 103 objects) are indicated by arrows. The dotted lines indicate constant luminosity ratios of $\alpha_{ox} = 1.2, 1.5$ and 1.9 , respectively. It shows that for most of the objects l_x roughly scales with l_o over about two orders of magnitudes, though with large scatter. Outliers are two objects with $\alpha_{ox} > 1.9$, showing much weaker X-ray emission by a factor of ~ 10 than expected for objects with $\alpha_{ox} = 1.5$, which is roughly the mean α_{ox} value.

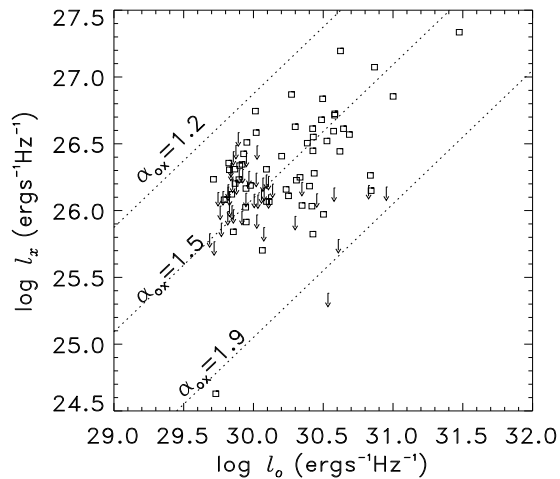


Fig. 8. The relation between the monochromatic l_x and l_o for the subsample in the redshift range $0.3 < z < 0.4$. Detections are indicated by squares and X-ray upper limits by arrows. The dotted lines indicate constant X-ray-to-optical luminosity ratios of $\alpha_{ox} = 1.2, 1.5$, and 1.9 , respectively.

Various methods of regression analyses were applied to determine the slope of the correlation $l_x \sim l_o^e$, taking into account upper limits, errors in one or both variables and/or assuming an intrinsic dispersion of the data. We obtained slopes ranging from ~ 0.7 to ~ 1.2 depending on the applied mathematical method and the analyzed data set (see the discussion of this problem in Babu & Feigelson 1996). For the analysis of the subsamples in different redshift bins the typical 1σ errors are $\Delta e \sim 0.2$, due to the small sample sizes.

Table 4. Regression analysis for the total quasar sample

Method ^{a)}	Δx	Δy	e	Source code
OLS	no error	no error	0.75 ± 0.03	IDL/Num.Rec.
OLS	no error	$\Delta l_x = 1\sigma$	0.814 ± 0.002	IDL/Num.Rec.
OLS	no error	$\Delta l_x = 0.3$	0.75 ± 0.01	IDL/Num.Rec.
ODR	$\Delta m = 0.2^b)$	$\Delta l_x = 1\sigma^c)$	1.00 ± 0.07	FV, $\sigma = 0$, fixed
ODR	$\Delta m = 0.2$	$\Delta l_x = 0.3$	0.91 ± 0.07	FV, $\sigma = 0$, fixed
ODR	$\Delta m = 0.2$	$\Delta l_x = 1\sigma$	1.16 ± 0.03	FV, $\sigma = 0.23 \pm 0.02$
ODR	$\Delta m = 0.2$	$\Delta l_x = 0.3$	1.15 ± 0.03	FV, $\sigma = 0.22 \pm 0.02$

^{a)} OLS: ordinary least squares regression, ODR: orthogonal distance regression

^{b)} Errors in optical luminosities are calculated assuming $\Delta m_v = 0.2$ magnitudes

^{c)} Errors in X-ray luminosities are either the 1σ statistical errors or, for illustrative purposes, an assumed error of 30% to account for possible systematic uncertainties.

For illustrative purposes we present in Table 4 the results of various methods for the determination of e for the total sample of the detected radio-quiet quasars (objects with $\alpha_{ox} > 2$ were excluded). The results obviously depend on the applied method and on the errors of the individual data points. For a discussion of the methods see paper I. It has been argued (La Franca et al. 1995) that ODR methods yield more reliable results for data with errors in both variables. Further, we note that the modified orthogonal distance regression method (FV, Fasano & Vio 1988) shows that there is significant dispersion in the data indicating that there is not the same strict one-to-one correlation between the two variables for all of the objects. An explanation for this result could be that the quasar sample does not form a homogeneous group of objects or that, for example, the orientation of the quasar to the line of sight affects the correlation given that X-rays and optical flux do not show the same angular dependence.

5.2. The α_{ox} distribution

To find the intrinsic distribution of the X-ray loudness α_{ox} we used a maximum-likelihood method, the “detections and bounds” or DB method developed by Avni et al. (1980, 1995) which takes into account both detections and upper limits (lower limits for α_{ox}) for the non-detections. This method gives reliable results only for randomly distributed censored data. Although the X-ray flux limits for the non-detections are set by the limiting sensitivity of the RASS and are thus relatively uniform, the limits on X-ray-to-optical luminosity ratios are, however, roughly randomly distributed. We derive the normalized distribution of α_{ox} in 20 bins from $\alpha_{ox} = 0.4$ to 2.4 ($f_i(\alpha_{ox}), i = 1, \dots, 20; \sum_{i=1}^{20} f_i(\alpha_{ox}) = 1$), in a non-parametric way. Such an analysis has the advantage of being able to determine the shape of the distribution without further a priori assumptions. We restrict the analysis to a subsample of objects with optical B -magnitudes

brighter than 18.5 in order to include a considerable fraction of detections (see Fig. 2 for the magnitude dependent X-ray detection rate). In fact, for objects much fainter than $B \sim 18.5$, the X-ray fluxes expected from the typical range of α_{ox} for radio-quiet quasars are generally below the flux limit of the RASS. This would lead to highly biased and thus meaningless lower limits of α_{ox} for the non-detections. The subsample thus comprises 377 detections and 989 non-detections, with a detection rate of $\sim 30\%$.

Fig. 9 shows the normalized histogram of α_{ox} for the detections (open line) and the best estimated “unbiased” distribution function derived from the DB method taking into account the lower limits of α_{ox} for non-detections (shaded). For the 377 X-ray detected objects (when the method reduces to the conventional sample statistics) we find a mean $\langle \alpha_{ox} \rangle = 1.54 \pm 0.01$, a standard deviation $\sigma \sim 0.17 \pm 0.01$ ($\sigma^2 = \sum_{i=1}^{20} f_i(\alpha_{ox,i} - \langle \alpha_{ox} \rangle)^2$), and a skewness = $0.29^{+0.34}_{-0.40}$ ($\sum_{i=1}^{20} f_i(\alpha_{ox,i} - \langle \alpha_{ox} \rangle)^3 / \sigma^3$); while the resulting maximum likelihood distribution including the non-detections yields a mean $\langle \alpha_{ox} \rangle = 1.65 \pm 0.01$, a standard deviation $\sigma = 0.19 \pm 0.01$, and a skewness = $0.43^{+0.39}_{-0.27}$, with a tail towards higher α_{ox} (the uncertainties are at 68% confidence level for one interesting parameter; see Avni et al. 1980, 1995). The results also indicate a large dispersion in the α_{ox} distribution, as could already be inferred in § 3.2 from the detection of objects in the RASS over a relatively wide range of optical magnitudes.

Of particular interest is a small number of objects showing very weak X-ray emission at 2 keV compared to their optical luminosity, as mentioned in § 3.2 and § 5.1. In Fig. 10 we plot the distribution of α_{ox} for the detected $z < 0.5$ objects in the magnitude-limited subsample, in order to avoid the “normal” high α_{ox} values expected for large z for a flux-limited sample. It shows more clearly a tail towards higher α_{ox} , with six objects having $\alpha_{ox} > 2.0$. Further, there are two objects which were not detected but must have values of $\alpha_{ox} > 1.95$. These objects show

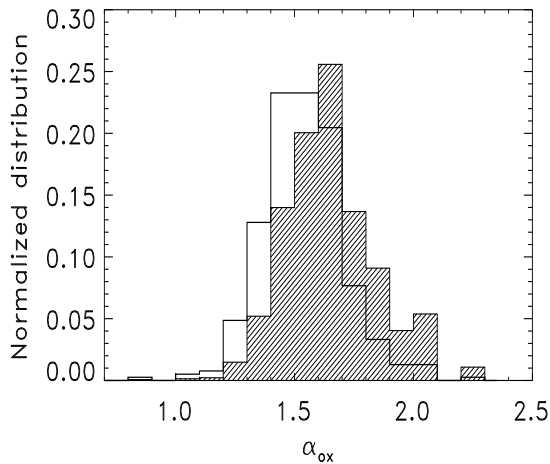


Fig. 9. Normalized distribution of the X-ray-to-optical luminosity ratios α_{ox} for the magnitude-limited subsample of objects with $B \leq 18.5$. The open line is for the objects detected in X-rays, and the shaded area represents the best estimate distribution taking into account non-detections using the maximum likelihood DB method (see the text).

highly reduced X-ray emission by more than a factor of 30 compared to the luminosities of the bulk of the detected objects at the same optical luminosity. These low redshift sources were detected in pointed observations only, except PG 0844+349 (at a high state) and PG 1001+05, which were also seen in the RASS. In fact, the non-detection of these objects in the RASS is the major cause of the reduced detection rate at bright magnitudes ($B \sim 15$) as shown in Fig. 2. Amongst the 20 nearby quasars with $z < 0.1$ in our optically selected sample, there are 3 of these “X-ray quiet” objects. The existence of “X-ray quiet” objects was also claimed by Laor et al. (1997) on the basis of 3 out of 23 objects, of which 2 are radio-quiet and included in our sample. It is not clear whether these objects are the X-ray quiet extremes of a continuous distribution or a distinct class of objects. We note, however, that X-ray variability might play a role in these objects; for example, PG 0844+349 appears to be “X-ray quiet” only in its low state. In addition, the possibility for some of them being previously unknown BAL objects, which remain undetected in soft X-rays (Green et al. 1995, Green & Mathur 1996), cannot be ruled out as well.

Excluding the 6 objects with $\alpha_{ox} > 2.0$ and the two objects with lower limits of $\alpha_{ox} > 1.95$, we obtained for the remaining 371 detected objects and 987 non-detections a slightly reduced mean and standard deviation ($\langle \alpha_{ox} \rangle = 1.63 \pm 0.01$, $\sigma = 0.16 \pm 0.01$), and a reduced best estimate for the skewness $= -0.12^{+0.48}_{-0.19}$, i.e., compatible with a symmetric distribution around the mean.

The such determined mean α_{ox} is consistent, within the mutual errors, with the values found in previous stud-

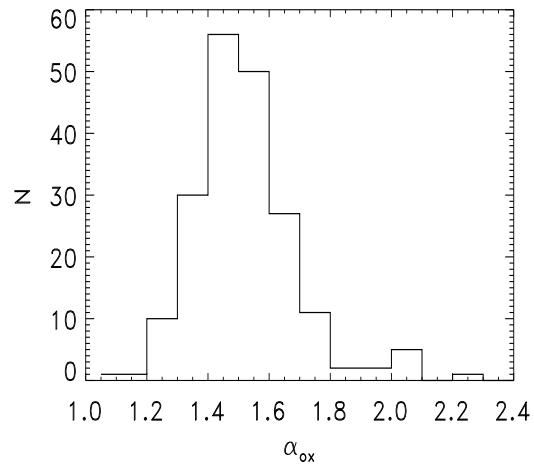


Fig. 10. Histogram of the α_{ox} distribution for objects with $z < 0.5$ from the magnitude-limited subsample. It shows a X-ray quiet tail towards higher α_{ox} .

ies (for example, $\langle \alpha_{ox} \rangle = 1.57 \pm 0.15$ for the LBQS sample with a limiting magnitude at $B \sim 19$, Green et al. 1995). The marginally higher best estimate arises from the brighter cut-off (18.5th mag) of our magnitude-limited subsample, as the observed α_{ox} appears to increase for high- l_o objects. The detection limit of the X-ray observations and the incompleteness of a sample affect the exact value of $\langle \alpha_{ox} \rangle$ as well. Finally, we used the relatively well determined individual spectral properties for many of the sources for the determination of the monochromatic X-ray luminosities instead of an overall spectral slope, which reduces the systematic uncertainties.

5.3. Dependence of α_{ox} on redshift and optical luminosity

We test the dependence of α_{ox} on z and l_o by applying both the non-parametric and parametric forms of the DB method to the magnitude-limited subsample. We excluded from the subsample the six objects with $\alpha_{ox} > 2.0$ and the two non-detections with lower limits $\alpha_{ox} > 1.9$ from the following analysis, for they show extremely weak X-ray emission compared to the bulk of the objects.

We first divided the subsample into six redshift bins, as defined in Table 5, in which the number of objects, the obtained $\langle \alpha_{ox} \rangle$ and standard deviations σ in each bin are listed. Beyond a redshift of $z = 0.5$, the $\langle \alpha_{ox} \rangle$ are consistent with one another within their mutual 1σ errors; whereas the $z < 0.2$ bin shows a significantly lower $\langle \alpha_{ox} \rangle$. The probability that the $z < 0.2$ bin has the same α_{ox} distribution as the higher redshift bins is less than $P < 0.01$. In fact, the mean α_{ox} in the $z < 0.2$ bin ($\langle \alpha_{ox} \rangle = 1.49 \pm 0.02$) is well determined, in the sense that all the objects were detected and the DB method is reduced to the conventional evaluation of the mean. The $\langle \alpha_{ox} \rangle$ for

the 126 detections in the $0.2 \leq z < 0.5$ bin is $\langle \alpha_{ox} \rangle \sim 1.53$, whereas the 90 undetected objects have an average lower limit of α_{ox} of ~ 1.57 . It is not clear from the analysis whether $\langle \alpha_{ox} \rangle$ depends primarily on z or on l_o , given the presence of a correlation between z and l_o for our magnitude-limited sample. We will investigate below whether at low redshifts ($z < 0.5$), $\langle \alpha_{ox} \rangle$ depends on both, z and l_o . The standard deviations of the α_{ox} distributions are consistent for all the z -bins.

Table 5. Maximum-likelihood α_{ox} distribution in redshift bins

redshift bins	N_d^a	N_b^b	$\langle \alpha_{ox} \rangle$	σ
$z < 0.2$	58	0	$1.49^{+0.02}_{-0.03}$	0.14
$0.2 \leq z < 0.5$	126	90	$1.60^{+0.02}_{-0.02}$	0.19
$0.5 \leq z < 1.0$	83	161	$1.63^{+0.04}_{-0.03}$	0.18
$1.0 \leq z < 1.5$	39	208	$1.69^{+0.02}_{-0.03}$	0.14
$1.5 \leq z < 2.0$	29	228	$1.68^{+0.06}_{-0.02}$	0.13
$z \geq 2.0$	36	299	$1.69^{+0.03}_{-0.03}$	0.15

Note: errors are at 68% confidence for 1 interesting parameter
a) number of objects detected in X-rays
b) number of objects with lower limits in α_{ox}

To investigate the $\alpha_{ox} - l_o$ dependence we divided the subsample into six $\log l_o$ bins, as defined in Table 6. The luminosity intervals were chosen such that the number of detections in a bin are roughly comparable. The derived $\langle \alpha_{ox} \rangle$ and 68% errors in all $\log l_o$ bins are listed in column 2 (case A) of Table 6, and are shown in Fig. 11, where the data points (only detections for clarity) are plotted. For comparison the “X-ray quiet” objects ($\alpha_{ox} > 2$, filled circles) are indicated as well. The mean α_{ox} shows a general increase with $\log l_o$; however, for low luminosities, $\log l_o \lesssim 30.5$, the $\langle \alpha_{ox} \rangle$ are consistent with being independent of $\log l_o$. This result is even more pronounced in case B (column 3 of Table 6), where the $z < 0.2$ objects with their significantly lower $\langle \alpha_{ox} \rangle$ were excluded to reduce the potential z dependences. The inclusion of the “X-ray quiet” objects does not affect the results. A similar trend of the $\alpha_{ox} - l_o$ relation has been noted by Avni et al. (1995) in a study of the *Einstein* quasar sample, and it can be inferred as well from the data of the radio-loud ROSAT quasars in paper I (Fig. 17) and those of the RASS-LBQS sample in Green et al. (1995, Fig. 4b).

The sample is large enough to allow an attempt for a non-parametric test for a joint α_{ox} dependence on both, l_o and z , in the $l_o - z$ plane. We subdivided the objects in each luminosity interval into four redshift ranges (distinguished by various symbols in Fig. 11), and list the obtained $\langle \alpha_{ox} \rangle$ in columns 4–7 of Table 6, respectively. An empty entry means that there are no or too few objects in the bin to yield reliable results. Although the binned

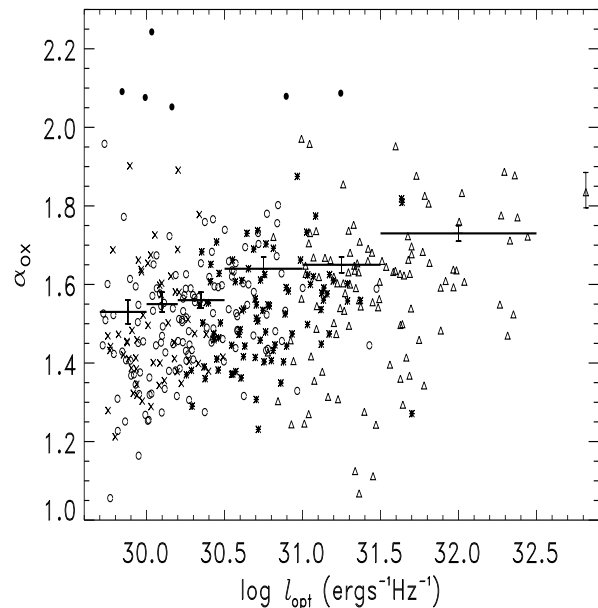


Fig. 11. The $\alpha_{ox} - \log l_o$ relation for the subsample of $B \leq 18.5$; only detections are plotted. The error bar at $\log l_o \sim 32.8$ indicates the typical 1σ error of the measured α_{ox} . The $\langle \alpha_{ox} \rangle$ and 68% errors, obtained by taking into account non-detections, are plotted for each $\log l_o$ bin. Plot symbols are: crosses for $z < 0.2$ objects; open circles for $0.2 \leq z < 0.5$ objects; asterisks for $0.5 \leq z < 1.0$ objects; triangles for $z \geq 1.0$ objects; filled circles for the “X-ray quiet” objects ($\alpha_{ox} > 2$).

data are too sparse to give statistically convincing results, a few conclusions can be inferred from the table: (a) In a given $\log l_o$ range the $\langle \alpha_{ox} \rangle$ at different z are consistent with each other within their mutual 1σ errors except for $\log l_o < 30$, where the $z < 0.2$ objects have a significantly lower (2σ confidence) $\langle \alpha_{ox} \rangle$ than in the $0.2 \leq z < 0.5$ range. This implies that the low $\langle \alpha_{ox} \rangle$ in the lowest- z bin ($z < 0.2$) found above arises from a true z -dependence at low redshifts, rather than as a consequence of a luminosity dependence. This redshift dependence is significant only for $\log l_o < 30$ objects. (b) For any redshift range the largest $\langle \alpha_{ox} \rangle$ is found in the highest $\log l_o$ bin though the significance is generally not high ($< 1.5 \sigma$), whereas the $\langle \alpha_{ox} \rangle$ in the other l_o bins of that redshift range are consistent with each other. This could imply that the $\alpha_{ox} - l_o$ dependence, found for the sample as a whole holds for every narrow redshift range.

In an alternative approach, we used the parametric form of the DB method (Avni & Tananbaum 1986, Wilkes et al. 1994) to fit a dependence of the form

$$\langle \alpha_{ox} \rangle = A_z[\tau(z) - 0.5] + A_o(\log l_o - 30.5) + A \quad (1)$$

to the data, where $\tau(z)$ is the look-back time in units of the Hubble time ($\tau(z) = 1 - (1 + z)^{-3/2}$ for $q_0 = 0.5$).

Table 6. Maximum-likelihood results for the mean $\langle\alpha_{ox}\rangle$ as a function of $\log l_o$ and z

$\log l_o$ $\text{erg s}^{-1} \text{Hz}^{-1}$	all redshifts		redshift ranges			
	case A ^{a)}	case B ^{b)}	$z < 0.2$	$0.2 \leq z < 0.5$	$0.5 \leq z < 1.0$	$z \geq 1.0$
$\log l_o < 30$	$1.53^{+0.03}_{-0.03}$	$1.58^{+0.06}_{-0.04}$	$1.47^{+0.04}_{-0.03}$	$1.58^{+0.06}_{-0.04}$	—	—
$30 \leq \log l_o < 30.2$	$1.55^{+0.03}_{-0.02}$	$1.57^{+0.07}_{-0.03}$	$1.51^{+0.03}_{-0.03}$	$1.55^{+0.06}_{-0.03}$	—	—
$30.2 \leq \log l_o < 30.5$	$1.56^{+0.02}_{-0.02}$	$1.58^{+0.05}_{-0.03}$	$1.52^{+0.05}_{-0.05}$	$1.59^{+0.07}_{-0.04}$	$1.57^{+0.04}_{-0.03}$	—
$30.5 \leq \log l_o < 31.0$	$1.64^{+0.03}_{-0.02}$	$1.64^{+0.03}_{-0.02}$	—	$1.70^{+0.10}_{-0.06}$	$1.60^{+0.03}_{-0.02}$	$1.66^{+0.18}_{-0.05}$
$31.0 \leq \log l_o < 31.5$	$1.65^{+0.02}_{-0.02}$	$1.65^{+0.02}_{-0.02}$	—	—	$1.75^{+0.14}_{-0.09}$	$1.64^{+0.02}_{-0.02}$
$\log l_o \geq 31.5$	$1.73^{+0.02}_{-0.02}$	$1.73^{+0.02}_{-0.02}$	—	—	—	$1.73^{+0.02}_{-0.02}$

Note: errors are at 68% confidence for 1 interesting parameter

a) using the magnitude-limited subsample

b) the same as a) but with $z < 0.2$ objects excluded

The fit assumes that the residuals of the α_{ox} have a Gaussian distribution. In Fig. 12 we show the joint 90% confidence contours for A_z and A_o (two interesting parameters) for the subsample (solid line), with the best estimates of $A_z = -0.016$ and $A_o = 0.11$. The results are consistent with those from the above non-parametric method and with previous studies (Kriss & Canizares 1985, Avni & Tananbaum 1986, Wilkes et al. 1994), showing a dependence of $\langle\alpha_{ox}\rangle$ on $\log l_o$, but not on redshift z . Excluding objects with $z < 0.2$ and $\log l_o < 30.0$, as mentioned above, leads to similar results (dotted line). Considering only low- z objects ($z < 0.5$), however, the contours (dashed line) show a slight dependence on z (an increase of α_{ox} by ~ 0.12 from the present epoch to half the Hubble time, i.e., $z \sim 0.6$, for the best fitted $A_z = 0.25$), at 90% confidence level, in addition to the dependence on $\log l_o$. The dependence of $\langle\alpha_{ox}\rangle$ on z at low redshifts ($z < 0.5$), found in a non-parametric way above, is confirmed.

In summary, our analyses show a dependence of α_{ox} on $\log l_o$ rather than on z . Two new features can be noted: up to $z \lesssim 0.5$, radio-quiet quasars, mostly the low- l_o objects ($\log l_o < 30$), show a slight increase in $\langle\alpha_{ox}\rangle$ with z . Secondly, the $\alpha_{ox} - \log l_o$ dependence is complex and the increase of α_{ox} with l_o is significant only for $\log l_o \gtrsim 30.5$.

It should be noted that the $z < 0.2$ objects have on average the lowest optical luminosities among the quasar population but higher than those of Seyfert I galaxies which have a mean $\langle\alpha_{ox}\rangle \sim 1.25$ (Kriss & Canizares 1985). Thus, our low- z , low- l_o sample might be contaminated by objects with quasar luminosities but still having Sy I - type properties. These objects would not be detected at higher redshifts and could thus lead to the observed $\langle\alpha_{ox}\rangle$ dependence with redshift.

Finally, the increase of $\langle\alpha_{ox}\rangle$ with $\log l_o$, inferred from the statistical analysis of the data, can not necessarily be interpreted as an intrinsic relationship of the quasar population. In paper I we have demonstrated that the apparent $\alpha_{ox} - \log l_o$ correlation can emerge even for an intrinsically uncorrelated sample, due to the inherent large

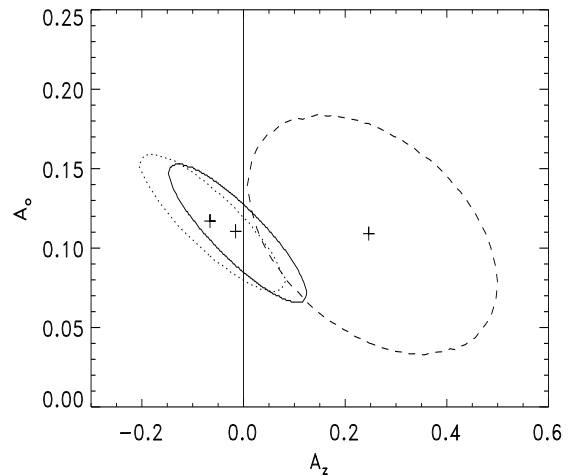


Fig. 12. The 90% confidence contours for the two parameters A_z and A_o of the $\alpha_{ox} - z, \log l_o$ dependence for the magnitude-limited subsample of $B \leq 18.5$, where the “X-ray quiet” objects ($\alpha_{ox} > 2$) have been excluded. Solid line: all objects; dotted line: all objects, but sources at $z < 0.2$ and $\log(l_o) < 30.0$ excluded; dashed line: objects at $z < 0.5$ only.

dispersion in the scaling law between l_x and l_o and the flux limitations of the observations, leading to a rhomboidal shaped phase space diagram (Fig. 19 of paper I). A detailed Monte Carlo simulation, addressing the question whether an underlying truly physical correlation can be extracted from the data in the presence of these biases will be presented elsewhere (Yuan et al. 1997).

6. Summary

We have presented the X-ray spectra and flux densities for 846 radio-quiet quasars detected by ROSAT in both the All-Sky Survey and in pointed observations. This is the largest sample of X-ray detected radio-quiet quasars

published so far, with many of the objects ($\sim 70\%$) being detected in X-rays for the first time. We studied the broad band properties of the population by using a sub-sample of optically selected, radio-quiet quasars from this compilation, which comprises 644 detections. The large number of objects enables us to investigate their properties in a wide range of parameter space with high statistical significance. Our major results are the following:

1. For radio-quiet quasars we found a systematically lower and much faster decreasing X-ray detection probability in the RASS towards faint optical magnitudes and high redshifts than for radio-loud objects (paper I). The on average higher X-ray luminosity of radio-loud quasars can account for these differences qualitatively.

2. A large fraction of the quasars, observed more than once in pointed observations, shows moderate flux variations, mostly by less than a factor of two. Extreme flux variations (by a factor of six) were found for only one radio-quiet object (PG 0844+349).

3. We confirm that radio-quiet quasars have in general steeper soft X-ray spectra ($\langle \Gamma_{gal} \rangle = 2.58 \pm 0.05$ for $z < 0.5$) than radio-loud objects ($\Delta\Gamma \sim 0.4$ and $\Delta\Gamma \sim 0.3$, compared to flat- and steep-spectrum radio quasars, respectively) and that this spectral difference persists at $z > 2$ with $\Delta\Gamma \sim 0.6$ compared to the flat-spectrum quasars (paper I). It is also confirmed that the soft X-ray spectra in the ROSAT band are systematically steeper than those in the harder *Einstein* IPC band by $\Delta\Gamma \sim 0.5$.

4. A spectral flattening with redshift is also confirmed for radio-quiet objects, which can be described by a linear relation of the form $\langle \Gamma_{gal} \rangle = 2.63(\pm 0.04) - 0.20(\pm 0.04) \times z$, for $z \lesssim 2.0$. As for the class of radio-loud quasars, the spectral slopes appear to be independent of redshift beyond $z \sim 2$. A decrease of the dispersion of the distribution of spectral slopes with redshift (from $\sigma = 0.38_{-0.04}^{+0.05}$ for $z < 0.5$ to $\sigma = 0.26_{-0.12}^{+0.20}$ for $z > 2.5$) is also inferred, though the significance is not high. These results are consistent with a composite X-ray spectral model including an additional steep soft X-ray component.

5. The spectral slope of $\Gamma \sim 2.23_{-0.19}^{+0.16}$ found for the ROSAT radio-quiet quasars at high redshifts ($z > 2.5$), is consistent, within the errors, with those found for nearby quasars in the medium energy X-ray band (2–10 keV) of $\Gamma \sim 2.0$. This implies that X-ray spectral evolution is not important in radio-quiet quasars. The steep spectra of radio-quiet quasars seen at $z > 2.5$ strengthen the claims that they cannot be the dominant contributors to the cosmic X-ray background.

6. The data are, in a statistical sense, consistent with no or only little excess absorption at all redshifts for radio-quiet quasars, though the significance of the result beyond $z \sim 2$ is not high.

7. By dividing the sample into narrow redshift bins ($\Delta z = 0.1$) for $z < 1$, the correlation between the X-ray luminosity and the luminosity at 2500\AA is explicitly tested and proved to be an intrinsic property of the

quasar population, though a large scatter is present in the correlation. The slopes of the regression line, obtained from different mathematical methods, cover a wide range, $0.7 \lesssim e \lesssim 1.2$. The existence of an intrinsic non-zero dispersion in the correlation between X-ray and optical luminosities suggest the existence of an additional “variable”, not accounted for in the analysis. One possibility would be a non-uniform, orientation dependent attenuation of the fluxes in the different energy bands.

8. In accordance with previous studies, the X-ray loudness α_{ox} seems to be independent of redshift but to correlate with $\log l_o$. The $\alpha_{ox} - \log l_o$ dependence is complex: the increase of α_{ox} with l_o is significant only for $\log l_o \gtrsim 30.5$ and the low- l_o radio-quiet quasars show a slight increase of $\langle \alpha_{ox} \rangle$ with z up to $z \lesssim 0.5$. However, this correlation might be primarily caused by luminosity selection biases and by the intrinsic dispersion of the data, as already discussed in paper I for radio loud quasars. A detailed study of these effects by Monte Carlo simulations will be presented elsewhere (Yuan et al. 1997).

9. Highly reduced X-ray emission, by more than a factor of ~ 30 compared to the bulk of the objects, is found in a few objects in the high- α_{ox} tail of the α_{ox} distribution. There are eight such “X-ray quiet” objects below $z < 0.5$, six detected by ROSAT and two upper limits, having $\alpha_{ox} > 2$. The reason for the low X-ray emission of these objects is unknown; we note, however, that X-ray variability might play a role. For example, the highly variable object PG 0844+349 is classified as “X-ray quiet” only in its low state.

Acknowledgements. The ROSAT project is supported by the Bundesministerium für Bildung, Wissenschaft, Forschung und Technologie (BMBF) and the Max-Planck-Gesellschaft. We thank our colleagues from the ROSAT group for their support, and M. Veron-Cetty for supplying a machine readable form of their catalogue. This research has made use of the NASA/IPAC Extragalactic Data Base (NED) which is operated by the Jet Propulsion Laboratory, California Institute of Technology, under contract with the National Aeronautics and Space Administration.

References

- Avni Y., Soltan A., Tananbaum H., Zamorani G., 1980, ApJ 238, 800
- Avni Y., Tananbaum H., 1982, ApJ 262, L17
- Avni Y., Tananbaum H., 1986, ApJ 305, 83
- Avni Y., Worrall D.M., Morgan, Jr. W.A., 1995, ApJ 454, 673
- Babu G.J., Feigelson E.D., 1996, *Astrostatistics*, Chapman and Hall, London
- Bechtold J., Elvis M., Fiore F., et al., 1994a, AJ 108, 374
- Bechtold J., Elvis M., Fiore F., et al., 1994b, AJ 108, 759
- Bischof O.B., Becker R.H., 1997 SISSA preprint
- Brinkmann W., 1992, in: Proc. of the Conference *X-ray Emission from AGN and the Cosmic X-ray Background*, MPE Report **235**, p. 143

- Brinkmann W., Yuan W., Siebert J., 1997, *A&A* 319, 413 (paper I)
- Brunner H., Friedrich P., Zimmermann H.-U., Staubert R., 1992, in *Proc. of the Conference X-ray Emission from AGN and the Cosmic X-ray Background*, eds. Brinkmann W., Trümper J., MPE Report **235**, p. 198
- Burstein D., Heiles C., 1978, *ApJ* 225, 40
- Canizares C.R., White J.L., 1989, *ApJ* 339, 27
- Cappi M., Matsuoka M., Comastri A., et al., 1997, *ApJ* 478, 492
- Dickey J. M., Lockman F. J., 1990, *ARA&A* 28, 215
- Elvis M., Wilkes B.J., McDowell J., 1991, in *Extreme Ultraviolet Astronomy*, eds. Malina R.F., Bowyer S., p.238
- Elvis M., Fiore F., Wilkes B.J., et al., 1994, *ApJ* 422, 60
- Fabian A.C., Barcons X., 1992, *ARA&A* 1992, 30, 429
- Fasano G., Vio R., 1988, *Newsletter of the Working Group for "Modern Astronomical Methodology"*, 7, 2
- Fiore F., Elvis M., McDowell J.C., et al., 1994, *ApJ*, 431, 515
- Gendreau K.C., Mushotzky R., Fabian A.C., et al., 1994, in *New Horizon of X-Ray Astronomy*, eds. Makino F., Ohashi T., Univ. Acad. Press, Tokyo, p. 365
- Green P.J., Schartel N., Anderson S.F., et al., 1995, *ApJ* 450, 51
- Green P.J., Mathur S., 1996, *ApJ* 462, 637
- Gregory P.C., Condon J.J., 1991, *ApJS* 75, 1011
- Gregory P.C., Vavasour, J.D., Scott, W.K., Condon, J.J., 1994, *ApJS* 90, 173
- Hasinger G., Burg R., Giacconi R., et al., 1993, *A&A* 275, 1
- Kellermann K.I., Sramek R., Schmidt M., et al., 1989, *AJ* 98, 1195
- Kriss G.A., Canizares C.R., 1985, *ApJ* 297, 177
- La Franca F., Franceschini A., Christiani S., Vio R., 1995, *A&A* 299, 19
- Laor A., Fiore F., Elvis M., Wilkes B., McDowell J.C., 1997, *ApJ* 477, 93
- LaValley M., Isobe T., Feigelson E.D., 1992, in *Astronomical Data Analysis Software and Systems*, eds. D.M. Worrall, C. Biemesderfer, J. Barnes, San Francisco, ASP Conf. Series Vol. 25, p.245
- Lawson A.J., Turner M.J.L., Williams O.R., Stewart G.C., Saxton R.D., 1992, *MNRAS* 259, 743
- Reimers D., Bade N., Schartel N., et al. , 1995, *A&A* 296, L49
- Maccacaro T., Gioia I. M., Wolter A., et al. , 1988, *ApJ* 326, 680
- Marshall H.L., Tananbaum H.T., Zamorani G., et al. , 1983, *ApJ* 269, 42
- Masnou J.L., Wilkes B.J., Elvis M., et al. , 1992, *A&A* 253, 35
- Mushotzky R., Done Ch., and Pounds K., 1993, *ARA&A* 31, 717
- Schartel N., Fink H., Brinkmann W., Trümper J., 1992, in *Proc. of the Conference X-ray Emission from AGN and the Cosmic X-ray Background*, eds. Brinkmann W., Trümper J., MPE Report **235**, p. 195
- Schartel N., 1995, PhD thesis, University of München
- Schartel N., Walter R., Fink H.H., Trümper J., 1996, *A&A* 307,33
- Schartel N., Komossa S., Brinkmann W., et al., 1997, *A&A* 320, 421
- Siebert J., Matsuoka M., Brinkmann W., et al., 1996, *A&A* 307, 8
- Stark A.A., Gammie C.F., Wilson R.W., et al. , 1992, *ApJS* 79, 77
- Stewart G.C., Georgantopoulos I., Boyle B., Shanks T., Griffiths R., 1994, in: *New Horizon of X-ray Astronomy*, Makino F., Ohashi T. (eds), Univ. Acad. Press, Tokyo, p.331
- Stocke J.T., Morris S.L., Weymann R.J., Foltz C.B., 1992, *ApJ* 396, 487
- Trümper J., 1983, *Adv. Space Res.*, 4, 241
- Turner J.J., Pounds K.A., 1989, *MNRAS* 240,833
- Ulrich M.-H., Molendi S., 1996, *ApJ* 457, 77
- Veron-Cetty M.-P., Veron P., 1993, *A Catalogue of Quasars and Active Nuclei (6th Edition)*, ESO Scientific Report No. 13 (VV93)
- Vignali G., Comastri A., Cappi M., Palumbo G.G.C., 1997, in *Proc. of the Conference From Micro to Mega Parsec*, 2nd Italian conference on AGN, Memorie S.A.IT
- Voges W., 1992, in *Proc. of the ISY Conference Space Science*, ESA ISY-3, ESA Publications, p.9
- Voges W., Gruber R., Paul J., et al., 1992, in *Proc. of the ISY Conference Space Science*, ESA ISY-3, ESA Publications, p.223
- Voges W., Gruber R., Haberl F., et al., 1995, *ROSAT NEWS* No. 32
- Voges W., Boller Th., Dennerl K., et al, 1996, in *Proc. of the Conference Röntgenstrahlung from the Universe*, eds. Zimmermann U., Trümper J., Yorke H., MPE Report **263**, p.637
- Walter R., Fink H.H., 1993, *A&A* 274, 105
- Wang T., Brinkmann W., Bergeron J., 1996, *A&A* 309, 81
- Wilkes B.J., Elvis M., 1987, *ApJ* 323, 243
- Wilkes B.J., Tananbaum H., Worrall D., et al., 1994, *ApJS* 92, 53
- Williams O.R., Turner M.J.L., Stewart G.C., et al., 1992, *ApJ* 389, 157
- Worrall D.M., Wilkes B.J., 1990, *ApJ* 360, 396
- Yuan W., Siebert J., Brinkmann W., 1997, submitted to *A&A*
- Zamorani G., Henry J.P., Maccacaro T., et al., 1981, *ApJ* 245, 357
- Zimmermann H.U., Becker W., Belloni T., et al., 1994, *EXSAS User's Guide*, MPE Report 257